Acta Geotechnica
https://doi.org/10.1007/s11440-024-02342-8

RESEARCH PAPER

An advanced ICMV for vibratory roller compaction

Johannes Pistrol[1] · Mario Hager[1] · Fritz Kopf[2] · Dietmar Adam[1]

Received: 21 September 2023 / Accepted: 9 April 2024

Abstract
The compaction success of vibratory roller compaction can be assessed by systems for continuous compaction control (CCC) or intelligent compaction (IC) which calculate soil stiffness-proportional quantities based on measurements of the motion behavior of the vibrating drum. However, state-of-the-art intelligent compaction meter values (ICMV) do not only depend on the stiffness of the soil but are also strongly influenced by machine and process parameters. In this paper, the methodology for determining an advanced ICMV is presented, in which the mechanical properties of the soil, the process parameters and geometric relationships in the contact area between the drum and the soil are directly included in the calculation. The methodology is explained on the example of measurement data from a compaction test conducted on sandy gravel with a heavy single-drum roller. The results of the novel ICMV are compared with those of the most widely used IC systems.

Keywords Continuous compaction control · Intelligent compaction · Nondestructive testing · Roller compaction · Soil dynamics

1 Introduction

Vibratory rollers are the primarily used machinery for near-surface compaction of granular media in earthworks. A vibratory roller uses a rotating-mass type of excitation in the axis of the drum to induce a predominantly vertical load transfer into the soil. The dynamically excited drum and the underlying soil form an oscillating interaction system with changing contact conditions. Different modes of operation of the interaction system may be observed, depending on the tuning of roller design parameters (dimensions of the drum, mass of the drum, axle load, unbalance moment, etc.), process parameters (e.g., excitation frequency, amplitude setting of the excitation, travel speed of the roller) and soil stiffness (grain size distribution, grain shape, water content, bedding density, loading history, etc.). If the drum remains in permanent contact with the soil, it operates in "continuous contact" [2]. In the event that the drum loses contact with the soil due to the dynamic excitation, Adam [2] distinguishes between the operating modes "partial uplift," "double jump," "rocking," and "chaos." "Partial uplift" with a periodic loss of contact at each revolution of the unbalance is the desired mode of operation, as it allows efficient compaction without excessive stress on the compaction equipment or the operator.

The characteristics of the motion behavior of the vibrating drum can be used to assess the compaction state of the soil or its load-bearing capacity. This basic idea has been used for decades by systems for continuous compaction control (CCC) and intelligent compaction (IC) [2, 3, 12, 14, 15, 24, 29].

In 1979, Thurner and Sandström found that the motion behavior of a vibrating drum depends on the stiffness of the soil. They used this finding to introduce the first system for CCC with vibrating rollers which enables a work- and

✉ Johannes Pistrol
johannes.pistrol@tuwien.ac.at

Mario Hager
hagma@gmx.at

Fritz Kopf
kopf@fcp.at

Dietmar Adam
dietmar.adam@tuwien.ac.at

[1] Institute of Geotechnics, TU Wien, Karlsplatz 13/220, 1040 Vienna, Austria

[2] FCP - Fritsch, Chiari & Partner ZT GmbH, Marxergasse 1B, 1030 Vienna, Austria

Published online: 04 May 2024

roller-integrated monitoring of the compaction process [24]. Since then, numerous research studies have been conducted to better understand the interaction between the vibrating drum of a vibratory roller [3, 17, 20, 27, 31] or an oscillatory roller [16, 18] and the soil.

The mechanics of the drum–soil interaction have for example been modeled by means of lumped parameter models [17, 25, 31] or cone models [2, 12]. All these studies assume a constant contact geometry between the drum and the soil.

In more recent research, dynamic elasto-plastic finite element models have been developed (e.g., [4, 5, 19]) to investigate the interaction between a vibrating drum and the soil. Kenneally et al. [11] already highlight the importance of the consideration of the variable contact geometry between the drum and soil in their FE analysis.

A most recent study [22] discussed the relevance of the variable contact geometry between vibrating drum and soil surface and introduced a simple mechanical model that enables the calculation of realistic force–displacement curves that are in good accordance with measurements.

Other recent studies primarily focus on the application of machine learning or artificial neural networks (ANNs) on intelligent compaction (e.g., [6]).

This paper describes the methodology for determining an advanced ICMV in which the mechanical properties of the soil, the process parameters and the geometric relationships in the variable contact area between drum and soil are directly included in the calculation.

1.1 Shortcomings of current ICMVs

The three leading systems for CCC/IC with vibratory rollers on the market, the Compactometer, the Terrameter and the ACE system with their four associated ICMVs—*CMV*, *OMEGA*, E_{vib} and k_{B}—differ in their procedure for signal evaluation and ICMV determination (e.g., frequency or time domain), their theoretical background and consequently also in their units [3, 14, 15, 24].

The different algorithms for determining the ICMVs are based either on empirically found correlations or on mechanical considerations (e.g., force–displacement diagram). The soil is assumed to have at most linear elastic material behavior. The contact geometry between drum and soil, if it is taken into account at all, is described by means of formulas for *Hertz*ian pressure and, in addition, the impact distance is kept constant during compaction. However, the variable drum contact width has a significant influence on the system reaction of roller and soil [22]. Likewise, the ratio of roller speed to excitation frequency (i.e., the impact distance) determines how much energy per unit length is introduced into the underlying soil layer.

Therefore, all mentioned and currently available ICMVs show a more or less pronounced dependence and sensitivity toward the prevailing soil conditions (e.g., water content), the selected process parameters (travel speed, excitation frequency and amplitude), the mode of operation of the drum, etc., so that all parameters that influence the motion behavior of the drum also show a significant influence on the readings of IC systems.

The current ICMVs are therefore not only influenced by the soil stiffness but also by the numerous roller and process parameters listed above. The guidelines governing the practical use of IC in earthworks take this into account in that all roller and process parameters must be kept constant during IC measurements for acceptance testing.

In addition, IC is an indirect measuring method for determining the compaction state of the soil and only provides relative values, partly without a physically justified background, which cannot be converted into each other under any circumstances. Rather, a calibration has to be performed for each roller–soil combination, in which the ICMVs are correlated with conventional testing methods in order to be able to finally relate them to the conventional compaction parameters used in contractual standards and regulations, such as the deformation modulus of static and dynamic load plate tests E_{v1}, E_{v2} or E_{vd}, or the degree of compaction D_{Pr}. This calibration process is time-consuming and often error-prone if untrained personnel are used.

All these circumstances underline the complexity of IC in the context of its practical application, especially when it comes to the correct interpretation of ICMV curves and the target-oriented application of IC in the sense of an areal compaction control. At the same time, the obvious need for further research and the desire for a new ICMV capable of compensating for the weaknesses of the existing ICMVs—not least in order to make IC more user-friendly in practice—becomes apparent.

On the basis of the optimization potential of current ICMVs, TU Wien and HAMM AG started a research project with the primary objective of developing an advanced ICMV for vibratory rollers.

1.2 Concept for the novel ICMV

During dynamic compaction with vibratory rollers, a characteristic motion behavior of the drum is established as a function of the soil properties. With the known machine parameters of the compaction device and the recorded motion behavior of the drum, the reaction force of the soil can be calculated [13]. Subsequently, a force–displacement diagram illustrating the relation between soil contact force and drum displacement can be determined in order to

derive parameters that provide relevant information about the compaction state of the soil. The measured soil response in the form of a force–displacement diagram is the first of five steps in the determination of the novel ICMV. This first step is a standard procedure that is already used by other IC systems [3, 14, 15]. The calculation of the soil contact force and the derived force–displacement diagram are explained in Sect. 3.

The challenging contact conditions between drum and soil surface characterize the dynamic interaction system of a vibratory roller [22]. In addition to the periodic or aperiodic loss of contact between drum and soil, the area between the two contact partners is a variable quantity during the loading phase, due to the cylindrically curved drum. A geometric model is introduced in the second step of the ICMV determination (Sect. 4) in order to account for the variable contact area between drum and soil. The measured motion behavior, already used for the measured soil response in the first step, is imposed on the geometric model in a path-controlled manner to determine the time-dependent width of the contact area between drum and soil while the length of the contact area is assumed to be constant and equal the length of the drum.

In the third step (Sect. 5), the measured motion behavior is applied on a Kelvin–Voigt model representing the soil. The spring stiffness and dashpot coefficient of the Kelvin–Voigt model are determined according to Wolf [30] but under consideration of the variable contact geometry obtained in the previous step. The variability of the contact geometry makes the spring stiffness and the dashpot coefficient time-dependent variables even when assuming a constant Young's modulus of the soil. The result of the third step is a theoretical soil response in the form of a force–displacement diagram.

By adjusting the parameters of the soil model characterizing the theoretical force–displacement diagram in the fourth step (Sect. 6), the best possible match between the theoretical and measured force–displacement diagrams can be found by means of a best-fitting process using suitable control criteria (target variables). Thereby, all control criteria represent characteristic variables of the force–displacement diagram which have a physical meaning and therefore, can be used as ICMV.

The parameter that best characterizes the stiffness of the compacted soil is its Young's modulus. Therefore, the Young's modulus of the mechanical soil model after the last iteration of the fitting process is adjusted to the static load from the measurements in a fifth and final step (Sect. 7). The resulting quantity is defined as novel ICMV for vibratory roller compaction and denoted by E_{geo}.

The novelty of the idea presented in this paper for the determination of the ICMV consists in the fact that both soil mechanical and geometrical parameters and correlations with direct physical meaning are directly included in the ICMV determination. Therefore, roller and process parameters as well as the modes of operation can be considered intrinsically to the system. Thus, the novel ICMV has the potential to be largely unaffected by changes in roller and process parameters (such as travel speed of the roller, frequency and amplitude of the excitation, direction of rotation of the unbalance, etc.) or modes of operation and thus to provide an absolute value mainly characterizing the soil stiffness with the corresponding unit of $\mathrm{MN/m^2}$. The methodology for determining the novel ICMV is explained using the example of experimental field tests with a HAMM single-drum roller.

2 Experimental field tests

The experimental field tests were carried out in a gravel pit near Vienna in 2019 as part of the joint research project between roller manufacturer HAMM AG and the Institute of Geotechnics at TU Wien. The extensive test program is not discussed in this paper, but is documented in [8].

The tests were carried out during an expansion of the gravel pit after the topsoil had been removed. Two test lanes, each 120 m long, were established on the surface of the sandy gravel layer of the gravel pit.

A HAMM H20i single-drum roller [9] was used for the tests. All machine parameters relevant for the ICMV calculation are given in Table 1; additional information can be found in [9]. The particular test referred to in this paper was performed with a large amplitude setting of the roller, an excitation frequency of $f = 25\,\mathrm{Hz}$ and a variation of the travel speed ($v = 2.5 - 4.0 - 6.0\,\mathrm{km/h}$) along the test lane.

The measuring system consisted of one-dimensional accelerometers with a sensitivity of $\pm 30\,\mathrm{g}$ mounted at the bearing of the drum. Accelerations were measured in horizontal direction of travel (x) and in vertical direction

Table 1 Roller parameters of the HAMM H20i single-drum roller used in the experimental field tests HAMM H20i technical data [9]

Roller parameter	Value
Diameter of the drum d	1.60 m
Length of the drum $2a$	2.14 m
Eccentricity of rotating mass e	0.0676 m
Rotating mass m_{e}	177.4 kg
Mass of the drum m_{d}	5590.6 kg
Mass of the frame m_{f}	6807.0 kg

(z) with a sampling rate of 10 kHz (see Fig. 1). In addition, relevant information of the CAN bus system was recorded, such as direction of travel, GPS data, amplitude setting, excitation frequency setting and travel speed.

3 Measured soil response

The novel ICMV for vibratory rollers is based on the soil response measured on the drum during compaction. The vibrating drum is considered as a rigid body—accelerations measured on one part of the drum are assumed to represent the motion of the entire drum. Accelerations have to be measured on an undamped part of the drum (e.g., the bearing). In the following, a parallel movement of the drum is assumed (same accelerations in the left and right bearing) to limit the required measurements to one side of the drum. However, the presented theory can be extended to account for a different motion behavior of the left and right side of the drum (like observed in a rocking mode of operation).

3.1 Calculation of the soil contact force *Fb*

The contact force F_b between the drum of the roller and the soil surface—which is defined positive for compression—comprises three main parts. Provided that there is sufficient dynamic decoupling between the drum and the frame, its vertical component is given by [2, 7, 13]:

$$\begin{aligned} F_b &= F_a + F_s - F_e \\ &= -m_d\, a_z + (m_d + m_f)g - m_e\, e\, \theta^2 \sin(\theta t + \phi) \end{aligned} \tag{1}$$

The inertia force F_a is determined by the measured vertical acceleration a_z in the bearing of the drum multiplied with the mass of the drum m_d (including the eccentric mass m_e). The static load F_s acting on the axis of the drum is the sum of gravitational forces caused by the mass of the drum m_d and the proportional mass of the frame on the axis m_f.

The magnitude of the centrifugal force resulting from the dynamic excitation is calculated from the eccentric mass m_e, its eccentricity e and the square of the angular excitation frequency θ (with $\theta = 2\pi f$). A multiplication of the centrifugal force by the sine of the phase angle, which comprises the angular frequency θ, the time t and the phase lag ϕ, gives the excitation force F_e.

The frequency f of the excitation results from the acceleration measured in the bearing of the drum. Therefore, the phase lag ϕ between the excitation (= centrifugal force or position of the eccentric mass, respectively) and the response (= drum movement or acceleration of the drum, respectively) remains the only unknown in Eq. 1.

For a lifted drum vibrating freely in the air without contact to the soil, the phase lag ϕ between the excitation force F_e and the response in the form of drum acceleration a_z is 180°. The phase lag ϕ deviates from 180° as soon as the drum interacts with the soil.

3.2 Force–displacement diagram based on measurements

A force–displacement diagram can be drawn for each period of excitation utilizing the soil contact force F_b and the vertical displacement s_z (see example in Fig. 2). This kind of diagram is already used for multiple ICMVs [3, 14, 15] and illustrates the reaction of the soil to the imposed movement of the drum (= resulting system response). The force–displacement relationship enables an analysis of energy, damping and stiffness characteristics for the compacted soil and therefore, provides information for the assessment of numerous compaction parameters:

The inclination of the hysteresis during loading and unloading phase can be associated with the stiffness and the state of compaction of the soil. The inclination of the unloading path is typically larger due to the compaction during the loading phase (plastic deformations of non-cohesive soil). Therefore, the soil behaves more rigidly during the unloading phase [23].

Since the unloading path does not match the loading path in the force–displacement diagram in Fig. 2, the dynamically excited drum transfers energy to the soil. The energy mainly comprises the radiation damping (=

Fig. 1 Measurement setup and definition of directions x and z in the experimental field tests (top), and photograph of the experimental field test (bottom)

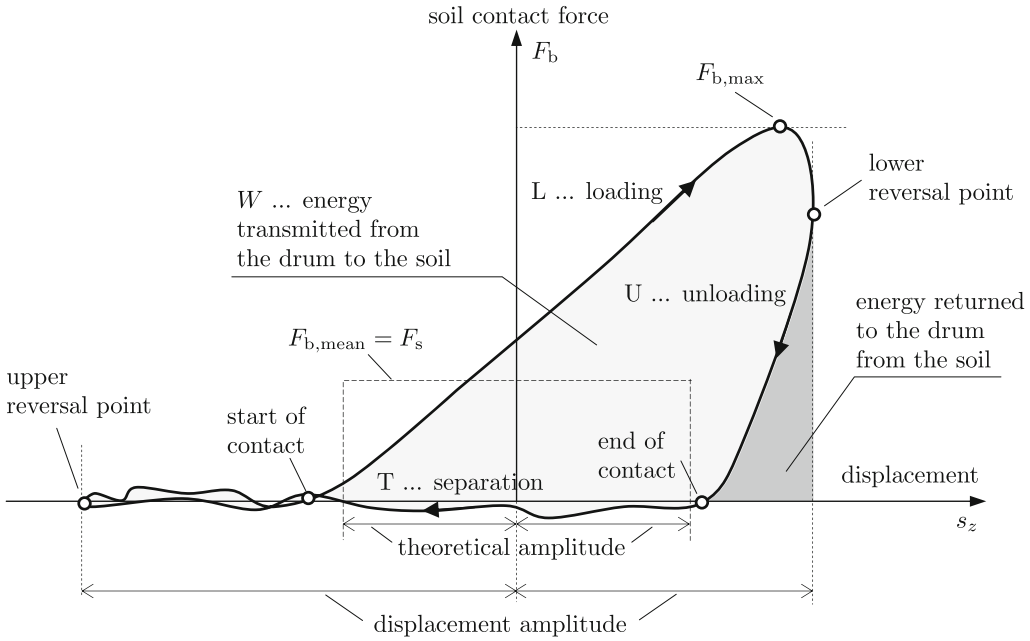

Fig. 2 Schematic representation of force–displacement diagram of the vibrating drum for mode of operation "partial uplift" [8]

geometric damping) and the performed compaction work. The material damping (grain-to-grain friction) and the energy converted to heat only play a minor role. The displacement of the force in the direction of action of compaction corresponds to the dynamic energy W transmitted into the soil. The area enclosed by the force–displacement relationship is thus a measure of the energy imprinted in the soil (light gray in Fig. 2). The dark gray area in Fig. 2 represents the portion of the generated roller energy that is returned to the drum from the soil.

The mean soil contact force $F_{b,mean}$ over one period of excitation (or two periods in case of mode of operation "double jump") has to equal the static load F_s. An integration of the temporal course of the soil contact force over one period of excitation (or two in case of "double jump") eliminates the components of acceleration and centrifugal force of the eccentric mass and also gives the static load F_s. The static load F_s and the magnitude of the excitation force F_e are usually known. Therefore, the above condition makes it possible to check the applicability of Eq. 1 for the calculation of the soil contact force F_b.

The maximum soil contact force $F_{b,max}$ and the points of start and end of contact obtained from the force–displacement diagram are additional parameters for the evaluation of the compaction process.

A force–displacement diagram as shown in Fig. 2 and its characteristics form the basis of the novel ICMV for vibratory rollers and all further steps for its evaluation presented in this paper. Up to this point, the method used state-of-the-art technology, which is also used for the determination of other ICMVs. Starting with Sect. 4, the methodology for the novel ICMV uses a different approach compared to previous studies. The new approach is explained on the example of measurement data obtained during the experimental field tests described in Sect. 2. Figure 3 shows the calculated soil contact force F_b (according to Eq. 1) from the experimental field tests over the vertical displacement s_z for eight periods of excitation. The vertical displacement s_z was not measured directly in the experimental field tests but is calculated from the acceleration measurements. A lowpass constrained least squares FIR filter of order 300, with a cutoff frequency of 300 Hz, a passband ripple of 0.01 dB and a stopband attenuation of 95 dB is applied on the measured acceleration signal. Offset adjustment is performed by subtracting the mean

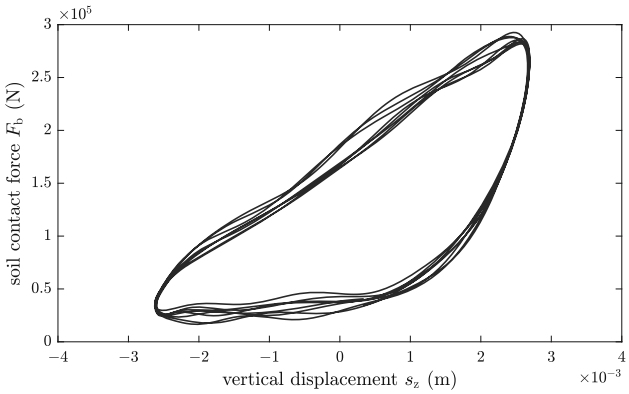

Fig. 3 Force–displacement diagram from measurements on the vibrating drum of a HAMM H20i single-drum roller

value from the signal. According to the recommendations in [10], the signal is then filtered again with a highpass butterworth IIR filter with a passband frequency of 8 Hz, a passband ripple of 0.001 dB, a stopband attenuation of 105 dB and a stopband frequency of 4 Hz. The cumulative integral of the signal over the time t is then computed via trapezoidal method followed by another offset adjustment and application of a highpass butterworth IIR filter with the same characteristics as before to obtain the vertical velocity v_z. Finally, the vertical displacement s_z is calculated by computing the cumulative integral of v_z, adjusting the offset and applying a highpass butterworth IIR filter with the same settings as before. It should be noted that the resulting vertical displacement s_z is a relative displacement and not the absolute displacement of the drum due to the numerical integration and offset adjustment described above.

4 Simulation for the determination of the contact area between drum and soil

The dynamic interaction between the drum of the roller and the soil is decisively characterized by the contact area between the two subsystems. While the length of the contact area (denoted by $2a$) may be assumed to equal the length of the drum, the contact width (denoted by $2b$) is a variable quantity in the course of the loading phase, due to the cylindrically curved drum and thus causes a significant non-linearity in the interacting system. During the loading phase, the drum increasingly penetrates the soil and the contact width between the two subsystems increases. After the drum reaches the lower reversal point of its motion, the contact width decreases again until it becomes zero and drum and soil move independently of each other during the loss of contact phase.

The simulation presented in the following is based on the measured motion behavior of the drum—taking into account the points of start and end of contact (see Fig. 2)—which is imposed in a path-controlled manner on a simplified geometric model to determine the contact geometry between the drum and the soil (see Figs. 4 and 5). The procedure is shown on the example of the "partial uplift" operating mode, as it is the desired mode of operation for compaction work with vibratory rollers. However, the considerations made can be applied analogously to the operating mode "double jump." With respect to the "continuous contact" operating mode, the presented method is limited, since there is no periodic loss of contact, no contact points can be identified and the contact width remains unknown at any time. However, the operating mode "continuous contact" only plays a minor role in vibratory roller compaction.

4.1 Input parameters of the simulation

The horizontal and vertical displacements x_M and z_M, respectively, of the drum center M describe the motion behavior of the drum (see Fig. 4). The horizontal displacement component x_M comprises the travel distance $x_\mathrm{d} = v\,t$ with speed v and the horizontal component of the vibratory excitation x_v, which equals the displacement s_x calculated from measurements. The vertical displacement component z_M corresponds to the displacement s_z from measurements. The movement of the drum center is thus defined by the measurements and already contains information about the speed of the roller v, the frequency of the excitation f—and thus also the impact distance $l_\mathrm{i} = v/f$ — as well as the direction of rotation of the eccentric mass. The upper and lower reversal points of the drum are given by the amplitude of the vertical drum displacement s_z (see Figs. 2 and 4). Note that the geometric relationships in Figs. 4 and 5 are not shown to scale—the impact distance l_i and the displacements x_M and z_M are over-scaled compared to the drum radius r.

In the first step, the contact points (start and end of contact) are identified in the force–displacement diagram (see Fig. 2) and assigned to the movement of the drum center in Fig. 4 resulting in the coordinates of the drum center for the start $(x_\mathrm{L}|z_\mathrm{L})$ and end $(x_\mathrm{U}|z_\mathrm{U})$ of contact. It is noted that the determination of these contact points is crucial in the simulation for the determination of the contact area and predefines the quality of the ICMV obtained from it. A mechanically balanced drum with synchronous oscillation (by means of a rigid body movement) is the basis for a sufficient identification of the contact points.

It is assumed that at the end of the unloading phase, i.e., at the time of the end of contact, the drum shape is imprinted in the soil and remains unchanged until the beginning of the next loading phase. From the knowledge of the contact points along the measured drum movement, the essential input parameters for the contact width simulation:

- the level of the subgrade before compaction z_u
- the level of the subgrade after compaction z_c
- the distance h_a of the uncompacted subgrade from the zero line
- the distance h_b of the compacted subgrade from the zero line

can be determined for each period of excitation using geometrical relations (see Fig. 4).

At the point of end of contact (drum center coordinates $x_\mathrm{U}|z_\mathrm{U}$), the drum looses contact to the soil and moves independently until it gets in contact with the soil again at the intersection $x_\mathrm{I}|z_\mathrm{I}$ of the uncompacted subgrade with the

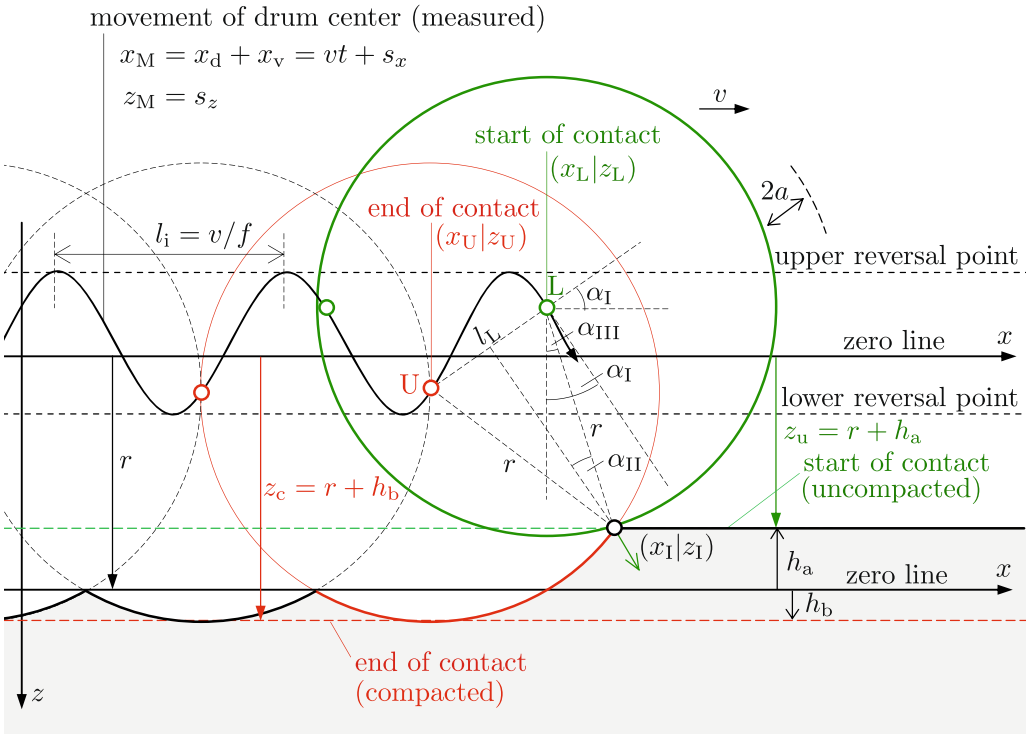

Fig. 4 Imposing the measured motion behavior of the drum on a simplified geometric model to determine the contact width $2b$. Illustration for the determination of the input parameters z_u, z_c, h_a and h_b of the simulation

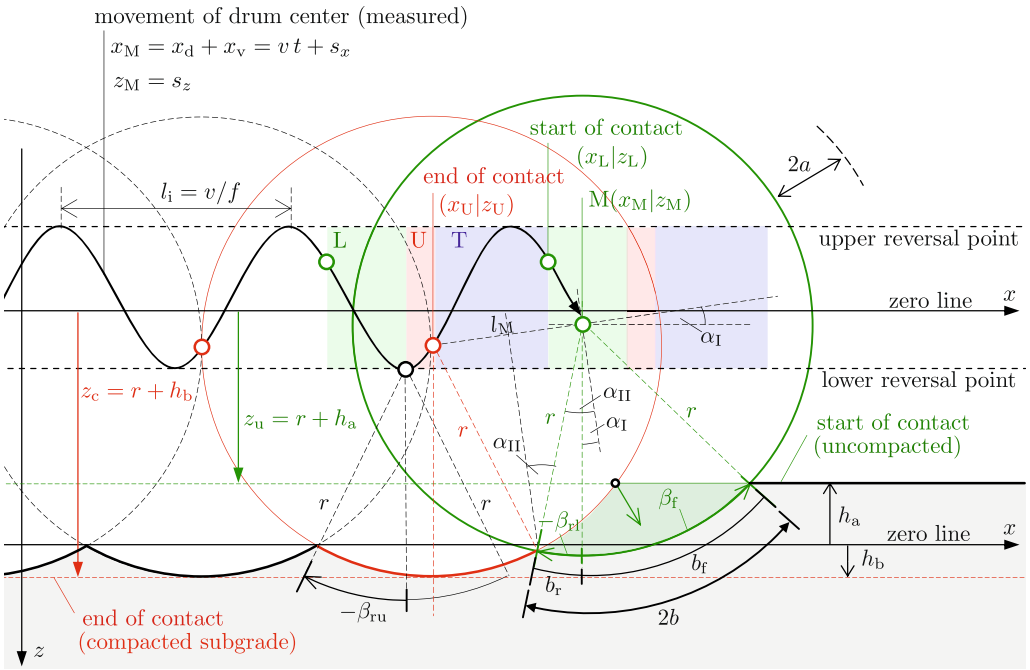

Fig. 5 Imposing the measured motion behavior of the drum on a simplified geometric model to determine the contact width $2b$. Operating phases: L = loading (green), U = unloading (red), T = separation (blue)

imprinted drum shape of plastic deformations from the previous load cycle at the beginning of the next loading phase (drum center coordinates $x_L|z_L$). The distance l_L between drum center positions at end of contact and start of contact is given by:

$$l_{\mathrm{L}} = \sqrt{(z_{\mathrm{U}} - z_{\mathrm{L}})^2 + (x_{\mathrm{L}} - x_{\mathrm{U}})^2} \tag{2}$$

The inclination of distance l_{L} is defined by the angle α_{I}:

$$\alpha_{\mathrm{I}} = \arctan\left(\frac{z_{\mathrm{U}} - z_{\mathrm{L}}}{x_{\mathrm{L}} - x_{\mathrm{U}}}\right) \tag{3}$$

Angle α_{II} (see Fig. 4) is:

$$\alpha_{\mathrm{II}} = \arcsin\left(\frac{l_{\mathrm{L}}}{2r}\right) \tag{4}$$

where r is the radius of the drum. The difference of the angles α_{I} and α_{II} is the angle α_{III} between the perpendicular through the center of the drum and the start of the contact at point I which is defined by its coordinates x_{I} and z_{I}. The horizontal and vertical distance between the drum center at contact start L and point I are given by:

$$\Delta x = r \sin \alpha_{\mathrm{III}} \tag{5}$$

$$\Delta z = r \cos \alpha_{\mathrm{III}} \tag{6}$$

The essential input parameters for the subsequent contact width determination in Sect. 4.2 are thus determined. They can be calculated as follows: Distance h_{b} of the compacted subgrade from the zero line:

$$h_{\mathrm{b}} = z_{\mathrm{U}} \tag{7}$$

Level of the subgrade after compaction z_{c}:

$$z_{\mathrm{c}} = r + h_{\mathrm{b}} \tag{8}$$

Level of the subgrade before compaction z_{u}:

$$z_{\mathrm{u}} = z_{\mathrm{I}} = z_{\mathrm{L}} + \Delta z = r + h_{\mathrm{a}} \tag{9}$$

Distance h_{a} of the uncompacted subgrade from the zero line:

$$h_{\mathrm{a}} = -(r - z_{\mathrm{u}}) \tag{10}$$

The level of the subgrade before compaction z_{u} (or the vertical distance of the soil surface h_{a} above the zero line) is significantly influenced by the speed of the roller v, the frequency of the excitation f, the horizontal vibration amplitude s_x and thus by the direction of rotation of the eccentric mass, as well as by the vertical coordinates of the points of start (z_{L}) and end (z_{U}) of contact. The level of the subgrade after compaction z_{c} (or the vertical distance h_{b} of the compacted subgrade from the zero line) mainly depends on the coordinates $(x_{\mathrm{U}}|z_{\mathrm{U}})$ of the end of contact point.

4.2 Determination of the contact width 2*b*

At the end of the unloading phase (drum center position U and red in Fig. 5), the level of the subgrade after compaction z_{c} is reached and the drum looses its contact to the soil. These end of contact points $(x_{\mathrm{U}}|z_{\mathrm{U}})$ are obtained from the measurements and it is assumed that the circular drum shape with the center of curvature at $(x_{\mathrm{U}}|z_{\mathrm{U}})$ gets imprinted to the subgrade by means of plastic deformations and remains unchanged until the beginning of the next loading phase. This results in an undulating subgrade after compaction, as shown in Figs. 4 and 5.

After the separation phase (T and blue in Fig. 5), in which the two subsystems move independently of each other, and at the beginning of the next load cycle, the drum hits the soil at the intersection of the level of the subgrade before compaction z_{u} with the imprint of the drum shape from the previous unloading phase (point I in Fig. 4) and penetrates into the subgrade again.

The drum with radius r and length $2a$ (which is assumed to be the length of the contact area) can now be imposed on the soil beginning at the start of contact $(x_{\mathrm{L}}|z_{\mathrm{L}})$ following the measured motion behavior and under consideration of the input parameters z_{c}, z_{u}, h_{a} and h_{b} obtained in Sect. 4.1. The procedure is shown in Fig. 5 for an arbitrary position of the drum center $(x_{\mathrm{M}}|z_{\mathrm{M}})$ during the loading phase and mode of operation "partial uplift."

Analogous to Eqs. 2 to 4, the distance l_{M} between the end of contact point and the current drum center position M, its angle of inclination α_{I} and the angle α_{II} can be computed:

$$l_{\mathrm{M}} = \sqrt{(z_{\mathrm{U}} - z_{\mathrm{M}})^2 + (x_{\mathrm{M}} - x_{\mathrm{U}})^2} \tag{11}$$

$$\alpha_{\mathrm{I}} = \arctan\left(\frac{z_{\mathrm{U}} - z_{\mathrm{M}}}{x_{\mathrm{M}} - x_{\mathrm{U}}}\right) \tag{12}$$

$$\alpha_{\mathrm{II}} = \arcsin\left(\frac{l_{\mathrm{M}}}{2r}\right) \tag{13}$$

For every point in time during loading, an angle β_{rl} between the vertical perpendicular through the drum center M and the intersection point of the drum at its current position and the imprinted shape of the previous load cycle is given by:

$$\beta_{\mathrm{rl}} = \alpha_{\mathrm{I}} - \alpha_{\mathrm{II}} \tag{14}$$

where the sign of β_{rl} is defined by Fig. 5.

As soon as the drum reaches its lower reversal point, the drum movement changes from loading to unloading (transition from green (L) to red area (U) in Fig. 5). The angle β_{ru} at this point in time between the direct line from the intersection point of the drum and the drum shape from the previous load cycle to the drum center and the vertical perpendicular through the drum center has a negative sign according to Fig. 5 and is defined as:

$$\beta_{ru} = -\arccos\left(\frac{z_c - z_M}{r}\right) \tag{15}$$

The drum subsequently moves upward and out of the soil again. Therefore, the angle β_{ru} decreases in magnitude until contact is finally lost and the drum contact width $2b$ thus becomes zero.

Both angles, β_{rl} and β_{ru}, describe the rear part of the contact width. Analogous, at every point in time during loading and unloading, an angle β_f can be identified between the vertical perpendicular through the drum center M and the intersection point of drum and subgrade before compaction z_u to define the front part of the contact width:

$$\beta_f = \arccos\left(\frac{z_u - z_M}{r}\right) \tag{16}$$

The entire contact width $2b$ is the sum of its front part b_f and rear part b_r. It is computed according to Eq. 17 under consideration of the definition of sign for the angles in Fig. 5:

$$2b = r(\beta_f - \beta_r)$$
$$\text{with } \beta_r = \begin{cases} \beta_f & \dots \text{for T} \\ \beta_{rl} & \dots \text{for L} \\ \beta_{ru} & \dots \text{for U} \end{cases} \tag{17}$$

According to Eq. 17, the rear part of the contact width b_r is defined in dependence of the operating phase by the angles β_f (separation, T), β_{rl} (loading, L) and β_{ru} (unloading, U), respectively. The front part of the contact width b_f is solely defined by the angle β_f. The maximum contact width is reached at the lower reversal point of the drum, when the operating phase changes from loading to unloading (see Fig. 5).

The result of the presented simulation is the development of the contact width $2b$ over time. Figure 6 gives an example obtained from the experimental field tests and shows the contact width $2b$ and its components b_f and b_r for the same eight periods of excitation already used in Fig. 2. The development of the contact width $2b$ for the entire compaction test is shown in Fig. 7 which clearly illustrates the influence of the roller speed on the contact width.

The simulated contact width, which is based on field measurements and assumptions presented in this section, serves as an important basis for the soil mechanical considerations in the following section.

5 Theoretical soil response

In the next step, a simple mechanical model is introduced to assess the theoretical soil response and simulate a theoretical force–displacement relationship. The measured drum movement is applied on the mechanical model under consideration of the contact area obtained in Sect. 4 to calculate a theoretical force–displacement diagram for each period of excitation.

The soil model is based on considerations by Wolf [30]. The contact area between drum and soil (denoted by its half side lengths a and b) is converted into a circle of equal area to represent the top surface of a half-infinite truncated cone. The simplification of the cone model is the consideration of only one-dimensional waves causing vertical radiation into the homogeneous subsoil with constant velocity. In [30] Wolf approximates the behavior of the truncated cone by a Kelvin–Voigt element. The description of the soil with a Kelvin–Voigt element is not sufficient to

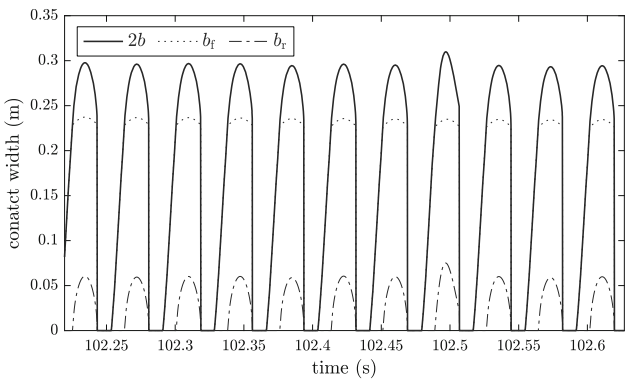

Fig. 6 Contact width $2b$ and its components for eight periods of excitation of the experimental field tests with a HAMM H20i single-drum roller

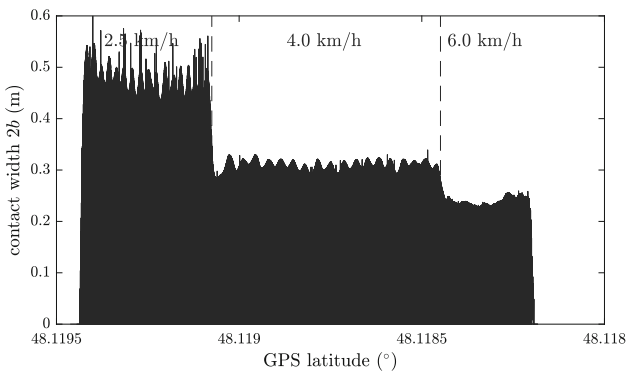

Fig. 7 Contact width $2b$ for the entire length of the test lane of the experimental field tests with a HAMM H20i single-drum roller

account for the soil behavior during a compaction process. Higher order material models are required to actually capture dynamic processes in the soil during vibratory roller compaction (e.g., hypoplasticity [26]). However, the main goal in the presented application is the modeling of a soil response at a certain state of compaction to calculate a theoretical soil reaction force resulting from the imprinted (measured) drum deflection. The calculated soil contact force provides information on the state of compaction and is used to determine a theoretical force–displacement diagram. This kind of application, as well as the predominantly vertical load transfer in vibratory roller compaction justifies the simplifications associated with the cone model.

The dynamic parameters representing the elastic isotropic half space of the cone, the elastic spring stiffness k and the parameter of the purely viscous dashpot c, both depend on the variable contact area between drum and soil and are given by [30]:

$$k = \frac{G\,b}{1-\nu}\left[3.1\left(\frac{a}{b}\right)^{0.75}+1.6\right] \tag{18}$$

$$c = \kappa\, 4\sqrt{2\rho\, G\frac{1-\nu}{1-2\nu}a\,b} \quad \text{(adapted)} \tag{19}$$

with:

$$G = \frac{E}{2(1+\nu)} \tag{20}$$

where G, ν and ρ are the shear modulus, Poisson's ratio and density of the soil, respectively. The dashpot coefficient in Eq. 19 covers the geometric damping (radiation damping) in the far field. Material damping in the near field is not taken into account due to its minor relevance [1]. Previous investigations [2, 12, 18] pointed out that an increase of the dashpot coefficient obtained from the cone model by a factor κ is required to account for spatial effects.

By estimating the density ρ and the Poisson's ratio ν of the soil and specifying a shear modulus G, the two variable parameters k and c can be determined for the variable contact width $2b$ obtained in Sect. 4 by means of Eqs. 18 and 19.

Combining the soil parameters from the cone model k and c with the displacement s_z and velocity v_z of the drum obtained from the measurements gives the forces F_k and F_c in the spring and dashpot, respectively, of the Kelvin–Voigt element:

$$F_\mathrm{k} = k s_z \tag{21}$$

$$F_\mathrm{c} = c v_z \tag{22}$$

The material behavior modeled with Wolf's cone model is linear elastic and therefore, not able to capture the compaction effect; a vibratory roller has on non-cohesive, compressible soils. Compaction is associated with plastic deformations by means of a reduction of the soil volume and void ratio, respectively, which yields to an increased soil density and bearing capacity.

For the unloading phase, an increased stiffness is used for the spring k of the Kelvin–Voigt element by introducing an unloading stiffness factor ξ to account for the compaction effect gained during the loading phase. This factor ξ considers the verifiable increase in spring stiffness k during the unloading phase and thereby, enables the consideration of permanent plastic deformations of the soil caused during the loading phase (material non-linearity) and represents a physical indicator for the description of the state of compaction.

The calculation of ξ for each period of excitation is based on the fact that the soil contact force F_b has to equal zero at the change from the unloading phase to the separation phase. A soil contact force $F_\mathrm{b} = 0$ in turn requires its components, the spring force F_k and the force in the dashpot F_c, to cancel each other out at this point in time (see Fig. 9). The force F_k in the elastic spring during unloading can be determined by Eq. 23:

$$F_\mathrm{k} = \xi k s_z \tag{23}$$

Figure 8 shows the temporal course of the adapted spring stiffness ξk and the dashpot coefficient c for eight periods of excitation, calculated from the variable contact geometry $2a\,2b$ presented in Fig. 6.

The theoretical soil contact force F_b (blue line in Fig. 9) is the sum of the adapted spring force F_k (red line in Fig. 9)—distinguishing between the loading phase (Eq. 21) and the unloading phase (Eq. 23)—and the force F_c in the viscous damper (magenta line in Fig. 9).

Imprinting the measured motion behavior of the drum (see Sect. 3) with the associated contact area simulated in Sect. 4 on a suitable soil model, yields to a system response by means of a theoretical soil contact force F_b. The temporal course of the theoretical soil contact force $F_\mathrm{b,S}$ and its components F_k and F_c are shown in Fig. 10 for the same eight periods of excitation used before. Analogous to the measured force–displacement diagram in Fig. 3, the theoretical soil contact force obtained in section 5 can thus be used to determine a theoretical force–displacement diagram for each period of excitation (see Fig. 11). It should be noted that the vertical displacement s_z is exactly the same for the measured and the theoretical soil response.

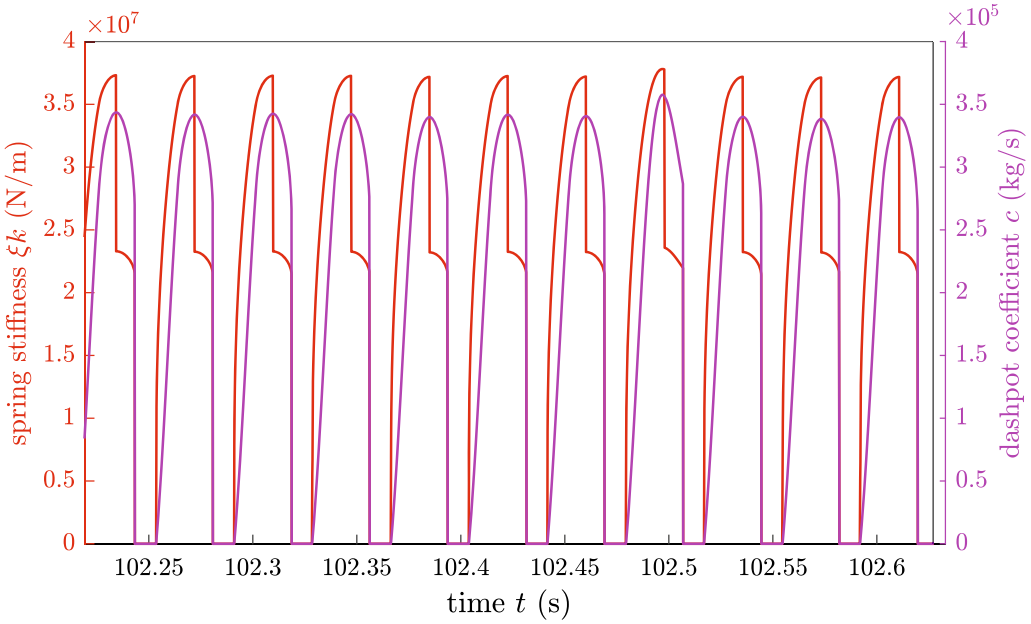

Fig. 8 Modified spring stiffness ξk and dashpot coefficient c for eight periods of excitation of the experimental field tests with a HAMM H20i single-drum roller

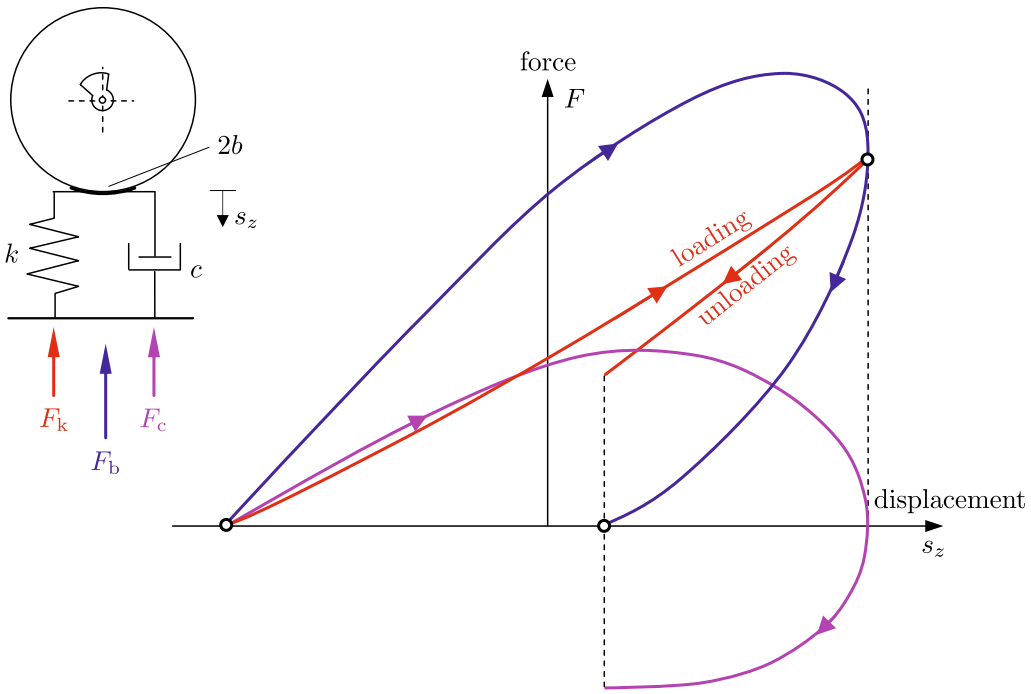

Fig. 9 Generating a theoretical force–displacement diagram based on a simple soil model: determination of the soil response on the imposed, measured motion behavior of the drum under consideration of the contact width for mode of operation "partial uplift"

6 Matching theory to measurement

The theoretical force–displacement diagram computed in Sect. 5 is based on measured data like drum displacement s_z and velocity v_z as well as the simulated development of the contact area which is also calculated from measured data. However, some parameters (e.g., Young's modulus E and density ρ of the soil, and damping factor κ) have to be assessed or defined to determine the theoretical soil contact force $F_{\mathrm{b,S}}$ and the corresponding diagram depicted in Fig. 11.

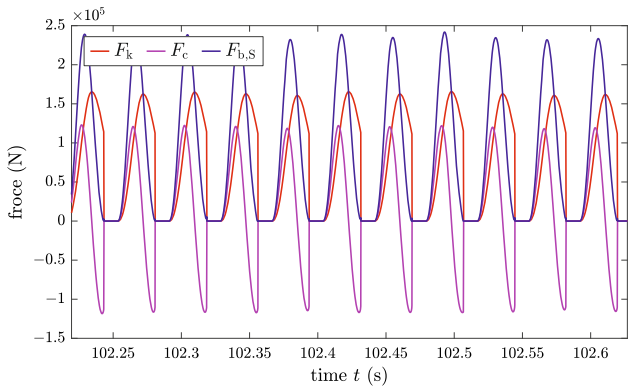

Fig. 10 Theoretical soil contact force $F_{b,S}$ and its components F_k and F_c for eight periods of excitation of the experimental field tests with a HAMM H20i single-drum roller

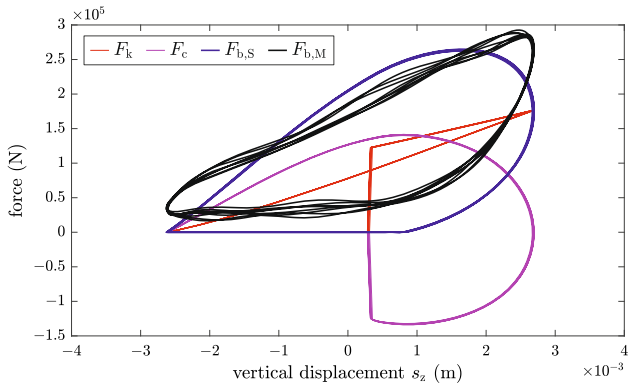

Fig. 11 Theoretical force–displacement diagram based on the simulation of the contact area between drum and soil and initial conditions of the mechanical soil model

In order to find the best possible match between the measured and the theoretical force–displacement diagram, the aforementioned parameters are varied by means of a best-fitting process. Control criteria are introduced that have a clear physical relevance and at the same time describe both the measured and the theoretical force–displacement diagram. While there are several possible criteria, three obvious criteria are used in the following:

- the maximum soil contact force $F_{b,max}$
- the static load F_S (equals the mean soil contact force $F_{b,mean}$ of one period of excitation in "partial uplift" operating mode or two periods of excitation in "double jump" operating mode, respectively)
- the dynamic energy W transmitted into the soil (equals the area enclosed by the force–displacement relationship).

The matching of theory and measurement is achieved by a numerical variation of the Young's modulus E of the soil and the damping factor κ under consideration of the three control criteria and is performed until the best possible match is found, and the deviation of the two force–displacement relationships from each other becomes minimal (see Fig. 12).

The Young's modulus E of the soil has a dominant influence on the inclination of the force–displacement diagram (both, during loading and unloading) as well as the magnitude of the soil contact force and thus, mainly affects the control criteria for maximum and average soil contact force ($F_{b,max}$ and $F_{b,mean}$, respectively). The damping factor κ, on the other hand, has a significant influence on the effective dynamic energy W transmitted into the soil (i.e., the area enclosed by the force–displacement relationship) and therefore, is the leading parameter for an adjustment of the fullness of the theoretical force–displacement diagram.

The best-fitting procedure comprises various steps that are repeated until a sufficient match of the two force–displacement diagrams is achieved. The procedure is carried out for two periods of excitation T_e each to account for the mode of operation "double jump" and is explained in the following sections.

6.1 Determination of factors for the soil model

As stated before, the Young's modulus of the soil E has a significant influence on the inclination of the force–displacement diagram as well as the magnitude of the soil contact force F_b and hence, its maximum $F_{b,max}$. Therefore, the first iteration ($n = 1$) of the best-fitting process is used to determine a factor $P_{b(n)}$ to adapt the arbitrarily chosen initial Young's modulus $E_0 = 30\,\mathrm{MN/m^2}$ used in Eqs. 18 and 19 in order to fit the simulation to the maximum soil contact force $F_{b,max,M}$ obtained from the measurements.

$$\begin{aligned} P_{b(n)} &= \min \| F_{b,max,M} - F_{b,max,S} \| \\ &= \min \| \underbrace{\max(F_{b,M})}_{\text{Measurement}} - \underbrace{\max\left(F_k P_{b(n)} + F_c \sqrt{P_{b(n)}}\right)}_{\text{Simulation}} \| \end{aligned} \tag{24}$$

The resulting factor $P_{b(n)}$ enters linearly into the spring force component of the soil model (see Eqs. 18 and 24) and with its square root into the damper component (see Eqs. 19 and 24).

The damping factor κ introduced in Eq. 19 dominates the area enclosed by the force–displacement relationship, and thus, the effective dynamic energy W transmitted into the soil. Therefore, it can be used to adjust the fullness of the theoretical force–displacement diagram. A factor $P_{a(n)}$ is introduced to fit the energy W_S calculated for the theoretical force–displacement diagram to the energy W_M obtained from the measured diagram under consideration

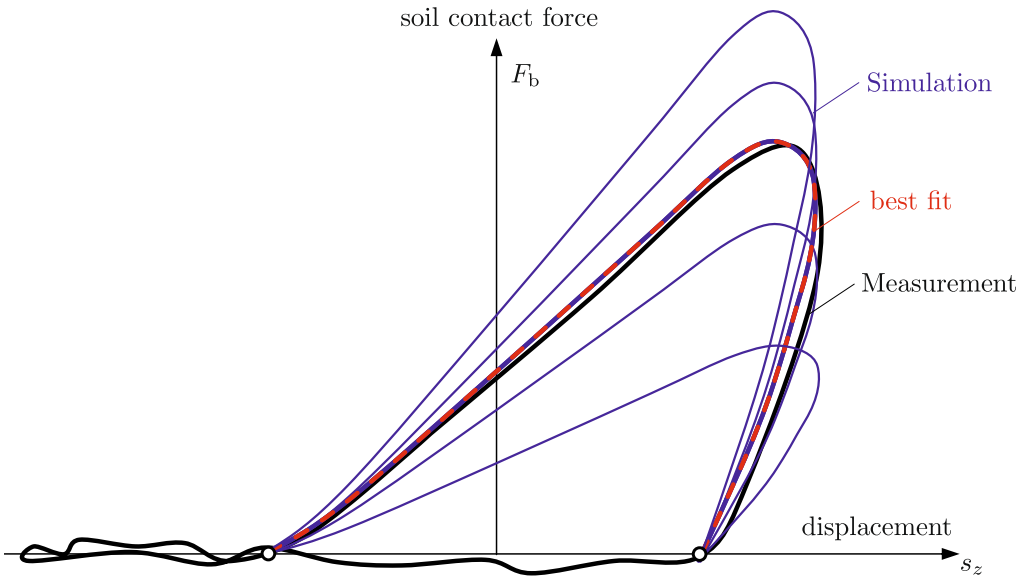

Fig. 12 Adapting the model parameters of the soil for a best possible match of simulated (blue) and measured (black) force–displacement diagram

of the factor $P_{b(n)}$ obtained in Eq. 24. $P_{a(n)}$ is a linear factor for the damping part in Eq. 25. For the example presented in this paper, an initial value of $\kappa_0 = 2$ is selected for the damping factor.

$$\begin{aligned} P_{a(n)} &= \min \|W_\mathrm{M} - W_\mathrm{S}\| \\ &= \min \| \int_{2Te} F_{\mathrm{b,M}} v_\mathrm{z}\, \mathrm{d}t - \int_{2Te} F_{\mathrm{b,S}} v_\mathrm{z}\, \mathrm{d}t \| \\ &= \min \| \underbrace{\int_{2Te} F_{\mathrm{b,M}} v_\mathrm{z}\, \mathrm{d}t}_{\text{Measurement}} \\ &\quad - \underbrace{\int_{2Te} \left(F_\mathrm{k} P_{b(n)} + F_\mathrm{c} P_{a(n)} \sqrt{P_{b(n)}}\right) v_\mathrm{z}\, \mathrm{d}t}_{\text{Simulation}} \| \end{aligned} \tag{25}$$

6.2 Modification of soil parameters

The initial values for the Young's modulus of the soil E_0 and the damping factor κ_0 used for the determination of the soil parameters k and c in Eqs. 18 and 19, respectively, are now factorized by the coefficients $P_{b(n)}$ and $P_{a(n)}$ obtained from Eqs. 24 and 25, respectively.

$$E_{(n)} = E_{(n-1)} P_{b(n)} \tag{26}$$

$$\kappa_{(n)} = \kappa_{(n-1)} P_{a(n)} \tag{27}$$

The updated values of $E_{(n)}$ and $\kappa_{(n)}$ serve as input parameters for the determination of the spring stiffness k in Eq. 18 and the dashpot coefficient c in Eq. 19 to rerun the simulation for the theoretical soil response presented in Sect. 5. The newly generated theoretical force–displacement diagram is the initial condition for the second iteration ($n = 2$) of the best-fitting process.

6.3 Iterations of the simulation

The two steps of the best-fitting process explained in Sects. 6.1 and 6.2 are repeated until the initial conditions of iteration n, $E_{(n)}$ and $\kappa_{(n)}$, match the parameters $E_{(n-1)}$ and $\kappa_{(n-1)}$ of the previous iteration step and the soil parameters k and c remain unchanged. According to Eqs. 28 and 29, this condition is satisfied when the factors $P_{b(n)}$ and $P_{a(n)}$ approach their limiting value close to 1, and thus, no further iteration step is required.

$$E_{(n)} \approx E_{(n-1)} P_{b(n)} \tag{28}$$

$$\kappa_{(n)} \approx \kappa_{(n-1)} P_{a(n)} \tag{29}$$

Figure 13 shows the initial values of the Young's modulus ($E_0 = 30\,\mathrm{MN/m^2}$) and the damping factor $\kappa_0 = 2$ for the entire test run and their change due to the best-fitting process. Both parameters, E and κ deviate significantly from the initial values after the first iteration ($n = 1$). The parameters after the third ($n = 3$) and fourth ($n = 4$) iteration are almost identical. The iteration process was therefore ended after the fourth iteration.

Figure 14 shows a comparison of the measured maximum of the soil contact force $F_{\mathrm{b,max,M}}$ with the results of the simulation after the first ($n = 1$) iteration ($F_{\mathrm{b,max,S,1}}$) and the fourth ($n = 4$) and final iteration ($F_{\mathrm{b,max,S,4}}$). The

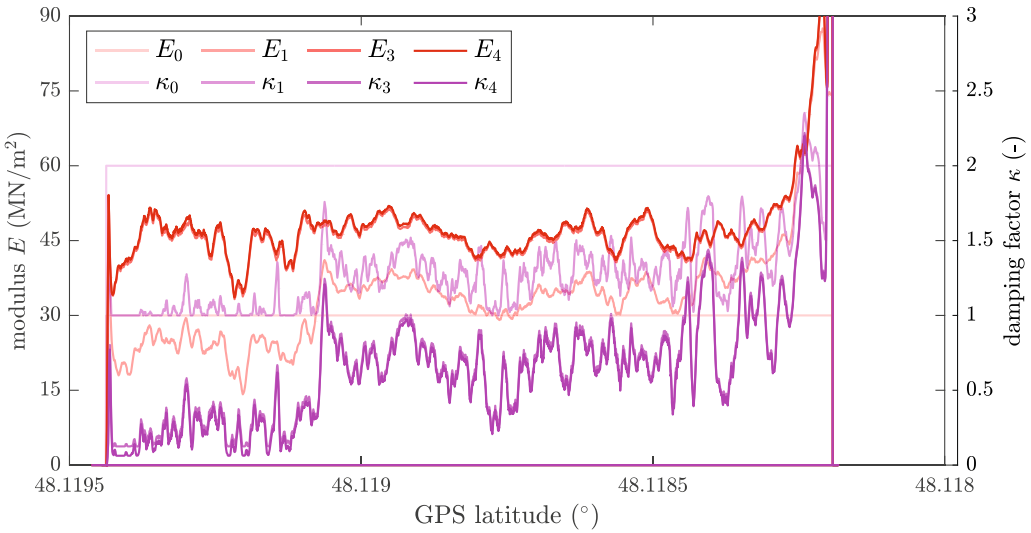

Fig. 13 Initial values of the Young's modulus (E_0) and the damping factor (κ_0) in comparison with the values obtained after the first ($n = 1$), third ($n = 3$) and fourth ($n = 4$) iteration of the fitting process

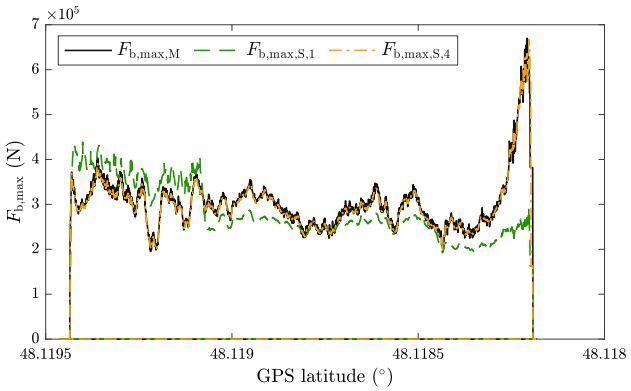

Fig. 14 Maximum soil contact force $F_{b,max}$ calculated from measurements in comparison with its simulated counterpart after the first ($n = 1$) and fourth ($n = 4$) iteration of the fitting process

difference of the maximum soil contact force between measurement and simulation is minimal (Eq. 24).

The result of fitting the simulated energy W_S to the energy calculated from measurements (W_M) is shown in Fig. 15. After the first iteration, the simulated energy still deviates significantly from the energy calculated from measurements. However, after the fourth and final iteration, the energy obtained from simulation is almost identical to the energy calculated from measurements (Eq. 25).

Figure 16 shows the force–displacement diagram from measurements for the same eight periods of excitation as in Fig. 11, but in comparison with the final results of the simulation after four iterations ($n = 4$) of the fitting process.

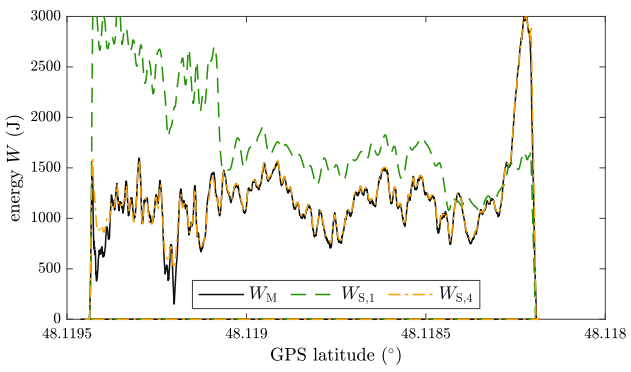

Fig. 15 Energy W transmitted into the soil calculated from measurements in comparison with its simulated counterpart after the first ($n = 1$) and fourth ($n = 4$) iteration of the fitting process

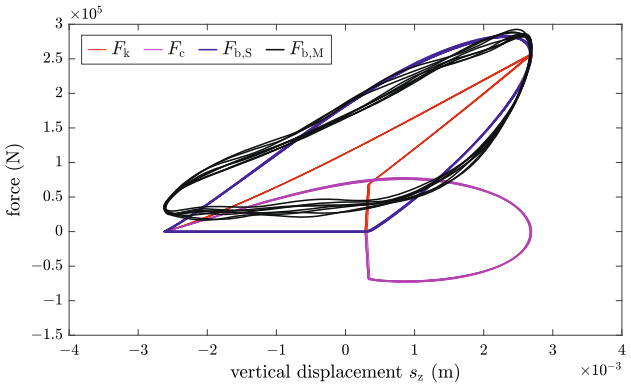

Fig. 16 Theoretical force–displacement diagram based on the simulation of the contact area between drum and soil after four iterations ($n = 4$) of the best-fitting process

7 Definition and application of the novel ICMV

In addition to its relevance for the inclination of the force–displacement diagram and the magnitude of the soil contact force, the Young's modulus of the soil has a significant influence on the mean soil contact force $F_{\mathrm{b,mean}}$ evaluated for two periods of excitation and thus on the static load F_{s}. Therefore, a final step in the best-fitting procedure is required to adjust the Young's modulus of the soil determined in Eq. 28, given the control criteria $F_{\mathrm{b,max}}$ and W by means of the factors $P_{b(n)}$ and $P_{a(n)}$, respectively, to the static load $F_{\mathrm{s,M}}$ resulting from the measurements.

$$E_{\mathrm{geo}} = E_{(n)} \frac{F_{\mathrm{s,S(n)}}}{F_{\mathrm{s,M}}} \tag{30}$$

According to Eq. 30, the Young's modulus $E_{(n)}$ resulting from Eq. 28 is factorized by the ratio of the static loads from the simulation $F_{\mathrm{s,S(n)}}$ and the measurements $F_{\mathrm{s,M}}$. The Young's modulus determined after the static load factorization is denoted by E_{geo} and defined as novel ICMV for vibratory roller compaction.

The novel ICMV has the unit of MN/m^2 and is the first of its kind to represent a purely soil stiffness-proportional quantity. In its determination both, geometrical and soil mechanical considerations are incorporated in a way that allows to account for machine and process parameters as well as operating modes—that all have a significant influence on other ICMVs—in a system-immanent way.

The individual steps for the calculation of the novel ICMV were explained on the example of measurement data from a field test conducted with a HAMM H20i single-drum roller (see Sect. 2). E_{geo} is evaluated for the entire pass of the roller and compared to the most common ICMVs—*CMV/RMV*, *OMEGA*, E_{vib} and k_{B}—in Fig. 17. The travel speed of the roller was increased ($v = 2.5 - 4.0 - 6.0\,\mathrm{km/h}$) during the test to investigate a potential influence of the travel speed on the ICMV reading.

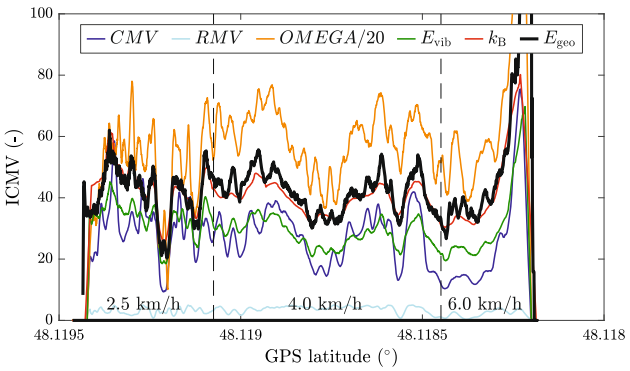

Fig. 17 Results of the novel ICMV E_{geo} in comparison with the readings of four established ICMVs for a test compaction with a HAMM H20i single-drum roller

Figure 17 shows that all investigated ICMVs (with the exception of *RMV*) show a qualitatively similar course along the test lane. However, differences in sensitivity, robustness and, of course, absolute values can be observed. *RMV* is not a stand-alone ICMV, but is supposed to be used in conjunction with the *CMV* in case of a "double jump" mode of operation [24]. The low values of *RMV* in Fig. 17 indicate that the roller operates in "partial uplift" mode and "double jump" does not occur.

E_{geo} shows an average magnitude of about 40 MN/m^2 and is able to capture the inhomogeneous conditions especially in the first third of the test lane. *CMV* and *OMEGA* show a stronger scatter of measured values, which makes the identification of weak spots more difficult. Moreover, the dependency of the ICMV on the travel speed of the roller is most pronounced for the *CMV*. The trend of E_{geo} is similar to that of E_{vib} and k_{B}, which are considered the most advanced ICMVs on the market [21].

8 Discussion

For the novel ICMV, the measured motion behavior of the drum is imposed on a simplified geometric model to determine the contact geometry between the drum of the roller and the soil. The presented approach enables a direct consideration of the impact distance in the calculation of E_{geo} and therefore limits the influence of the travel speed of the roller and the excitation frequency on the final ICMV reading. The determination of the contact geometry requires the identification of the start and end points of contact in the measured motion behavior. The following steps of the ICMV calculation greatly depend on an accurate identification of those points. Therefore, the presented methodology requires clean measurements on a mechanically balanced drum with synchronous oscillation (by means of a rigid body movement) for reliable and robust ICMV determination.

In its presented formulation, E_{geo} can be used for the "partial uplift" (desired) and "double jump" modes of operation. An extension of the geometric model to account for different motion behavior of the left and right sides of the drum could easily be implemented to also account for a "rocking" mode of operation. A clear limitation of E_{geo} is its applicability to soft soils when the roller is operating in "continuous contact." The contact points mentioned above do not exist in "continuous contact," and therefore, the contact geometry can only be assumed, but not calculated from measurements. Additional tests showed that E_{geo} gives reduced values in case of "continuous contact"; however, the obtained readings no longer have a physical meaning.

The simplified approach of modeling the soil by means of a spring-dashpot element and an unloading stiffness factor was deliberately chosen to allow the calculation of E_{geo} on a roller in real time. The concept can be easily extended should practical application show the need. Possible extensions are the consideration of a different motion behavior of the left and right side of the drum, higher order material models to represent the soil reaction and the introduction of alternative or additional control criteria for the optimization process.

E_{geo} is the Young's modulus of the simplified soil model used to determine the ICMV. However, it must not be misinterpreted as the actual Young's modulus of the soil. E_{geo} reflects only the stiffness of the soil under the harmonic loading of the vibrating drum and is therefore strain dependent. Vibration excitation of the same soil with a larger amplitude (increased F_e) would result in larger strains and yield a smaller E_{geo}. Future research and further development of E_{geo} could focus on implementing shear modulus degradation curves (an overview is given, for example, by Wichtmann and Triantafyllidis [28]) in the determination of the novel ICMV to compensate for the strain dependence of the resulting E_{geo}.

In this paper, only the methodology for the novel ICMV was presented and tested on a single set of measured data. Extensive experimental field tests with different roller types and sizes and varying process parameters as well as a comparison of E_{geo} with conventional spot-like tests are required to proof its potential.

9 Conclusions

In this paper, the methodology for the calculation of an advanced ICMV was presented that has the potential to overcome the drawbacks of current IC systems by directly considering machine and process parameters in the determination of the new measure.

For the novel ICMV, the measured motion behavior of the drum was imposed on a simplified geometric model to determine the contact geometry between the drum of the roller and the soil. The measured drum movement was then applied on a mechanical model representing the soil under consideration of the calculated contact geometry to determine a theoretical force–displacement diagram for each period of excitation. A best-fit procedure was used to adjust the elastic parameters of the soil model to fit the theoretical force–displacement diagram to the measured diagram, using the mean and maximum soil contact forces and the compaction energy as control criteria. The Young's modulus of the mechanical soil model after the optimization process factorized with the static load ratio was defined as novel ICMV for vibratory rollers and is denoted as E_{geo}.

The main findings of the research are as follows:

1. The consideration of the impact distance in the calculation of E_{geo} limits the influence of the travel speed of the roller and the excitation frequency on the final ICMV reading.
2. The presented methodology requires clean measurements on a mechanically balanced drum with synchronous oscillation for reliable and robust ICMV determination.
3. The good match of measured and theoretical soil response suggests that the selection of target and control variables of the best-fitting procedure is sufficient for the simulation to mirror the measured system behavior.
4. In its presented formulation, E_{geo} can be used for the "partial uplift" and "double jump" modes of operation but not for "continuous contact" which is relevant for very soft soils.
5. E_{geo} was evaluated for a compaction test conducted in the scope of experimental field tests with a heavy single-drum roller and compared with the results of four established ICMVs. For this test, E_{geo} does not show a dependence on the travel speed of the roller. The results are at least on par with established ICMVs.
6. The modular concept for the determination of E_{geo} can easily be extended. Possible extensions are the consideration of an asymmetric motion behavior of the drum, higher order material models to represent the soil response and the introduction of alternative or additional control criteria for the optimization process.
7. In this paper, the methodology for determining an advanced ICMV was presented using the example of a single measurement data set. To prove the potential of E_{geo}, extensive experimental field tests in conjunction with systematic sample point detection methods are required.
8. In its presented formulation, E_{geo} is a strain dependent modulus. Future research could implement shear modulus degradation curves to compensate for this strain dependence.

Acknowledgements The financial support by the manufacturer of compaction equipment HAMM AG, Hammstraße 1, 95643 Tirschenreuth, Germany, made this research possible and is gratefully acknowledged. The authors acknowledge TU Wien Bibliothek for financial support through its Open Access Funding Programme. This paper is dedicated to DI(FH) Werner Völkel (1953–2021), our friend and curious supporter of our work over many unforgettable years.

Funding Open access funding provided by TU Wien (TUW).

References

1. Adam C, Adam D (2003) Modelling of the dynamic load plate test with the light falling weight device. Asian J Civil Eng 4:73–89
2. Adam D (1996) Continuous Compaction Control (CCC) with vibrating rollers (in German). PhD thesis, TU Wien, Vienna, Austria
3. Anderegg R, Kaufmann K (2004) Intelligent compaction with vibratory rollers: Feedback control systems in automatic compaction and compaction control. Transp Res Rec 1868(1):124–134. https://doi.org/10.3141/1868-13
4. Cao Y, Huang X, Ma L, et al (2011) Finite element analysis to vibratory drum - Soil model of vibratory roller. In: Applied Mechanics and Materials, pp 2005–2008, https://doi.org/10.4028/www.scientific.net/AMM.94-96.2005
5. Cao Y, Xiang L, Ma L, et al (2013) Application analysis of vibrating wheel-soil model based on ABAQUS. In: Advanced Materials Research, pp 366–369, https://doi.org/10.4028/www.scientific.net/AMR.644.366
6. Fathi A, Tirado C, Rocha S et al (2021) A machine-learning approach for extracting modulus of compacted unbound aggregate base and subgrade materials using intelligent compaction technology. Infrastructures 6(10):142. https://doi.org/10.3390/infrastructures6100142
7. Grabe J (1993) Fortlaufend inverse Berechnung der Bodensteifigkeit aus dem Schwingungsverhalten einer fahrenden Vibrationswalze. Arch Appl Mech 63(7):472–478. https://doi.org/10.1007/BF00788045
8. Hager M (2022) CCC with Vibrating Rollers – Development of a new Indicator for Roller-Integrated Continuous Compaction Control (in German). PhD thesis, TU Wien, Vienna, Austria
9. HAMM AG (2019) H20i technical data. https://l-lynch.com/uploads/Product%20Specification%20Sheets/Lynch_HeavyRoller-Hamm-H20i.pdf
10. Hofmann S (2013) Numerische Integration von Beschleunigungssignalen. Mitteilungen aus dem Institut für Maschinenwesen der Technischen Universität Clausthal 38:103–114
11. Kenneally B, Musimbi OM, Wang J et al (2015) Finite element analysis of vibratory roller response on layered soil systems. Comput Geotech 67:73–82. https://doi.org/10.1016/j.compgeo.2015.02.015
12. Kopf F (1998) Continuous Compaction Control (CCC) during compaction of soil by dynamic rollers with different types of excitation (in German). PhD thesis, TU Wien, Vienna, Austria
13. Kröber W (1988) Investigation of the dynamic processes during the vibratory compaction of soils (in German). PhD thesis, Technische Universität München, Munich, Germany
14. Mooney M, Rinehart R (2007) Field monitoring of roller vibration during compaction of subgrade soil. J Geotech Geoenviron Eng 133(3):257–265. https://doi.org/10.1061/(ASCE)1090-0241(2007)133:3(257)
15. Mooney M, Rinehart R (2009) In situ soil response to vibratory loading and its relationship to roller-measured soil stiffness. J Geotech Geoenviron Eng 135(8):1022–1031. https://doi.org/10.1061/(ASCE)GT.1943-5606.0000046
16. Paulmichl I, Furtmüller T, Adam C et al (2020) Numerical simulation of the compaction effect and the dynamic response of an oscillation roller based on a hypoplastic soil model. Soil Dyn Earthquake Eng 132:106057. https://doi.org/10.1016/j.soildyn.2020.106057
17. Pietzsch D, Poppy W (1992) Simulation der Bodenverdichtung mit Vibrationswalzen. Bauingenieur 67(9):383–391
18. Pistrol J, Adam D (2018) Fundamentals of roller integrated compaction control for oscillatory rollers and comparison with conventional testing methods. Transp Geotech 17:75–84. https://doi.org/10.1016/j.trgeo.2018.09.010
19. Pistrol J, Falkner FJ, Adam D, et al (2012) Comparison of constitutive soil models for the simulation of dynamic roller compaction. In: ECCOMAS 2012 - European Congress on Computational Methods in Applied Sciences and Engineering, e-Book Full Papers, pp 5925–5939
20. Pistrol J, Adam D, Villwock S et al (2015) Movement of vibrating and oscillating drums and its influence on soil compaction. Geotech Eng Infrastruct Develop Proc XVI Eur Conf Soil Mech Geotech Eng ECSMGE 2015:349–354
21. Pistrol J, Hager M, Adam D (2022) CCC Systems for Vibratory and Oscillatory Rollers in Theoretical and Experimental Comparison. In: Tutumluer E, Nazarian S, Al-Qadi I, et al (eds) Advances in Transportation Geotechnics IV. Springer International Publishing, Cham, Lecture Notes in Civil Engineering, pp 217–229, https://doi.org/10.1007/978-3-030-77238-3_17
22. Pistrol J, Hager M, Kopf F et al (2023) Consideration of the variable contact geometry in vibratory roller compaction. Infrastructures 8(7):110. https://doi.org/10.3390/infrastructures8070110
23. Studer JA, Koller MG, Laue J (2008) Bodendynamik: Grundlagen, Kennziffern, Probleme und Lösungsansätze, 3rd edn. Springer-Verlag Berlin Heidelberg, Berlin, https://doi.org/10.1007/978-3-540-29625-6
24. Thurner H, Sandström Å (1980) A new device for instant compaction control. Int Conf Compact. France, Paris, pp 611–614
25. van Susante PJ, Mooney MA (2008) Capturing nonlinear vibratory roller compactor behavior through lumped parameter modeling. J Eng Mech 134(8):684–693. https://doi.org/10.1061/(ASCE)0733-9399(2008)134:8(684)
26. von Wolffersdorff PA (1996) A hypoplastic relation for granular materials with a predefined limit state surface. Mech Cohesive-frictional Mater 1:251–271
27. White D, Thompson M (2008) Relationships between In situ and roller-integrated compaction measurements for granular soils. J Geotech Geoenviron Eng 134(12):1763–1770. https://doi.org/10.1061/(ASCE)1090-0241(2008)134:12(1763)
28. Wichtmann T, Triantafyllidis T (2013) Effect of Uniformity Coefficient on G/Gmax and Damping Ratio of Uniform to Well-Graded Quartz Sands. J Geotech Geoenviron Eng 139(1):59–72. https://doi.org/10.1061/(ASCE)GT.1943-5606.0000735
29. Winter MG (2020) Continuous compaction control in the UK: History, current state and future prognosis. Proc Inst Civil Eng Geotech Eng 173(4):348–358. https://doi.org/10.1680/jgeen.19.00120
30. Wolf JP (1994) Foundation vibration analysis using simple physical models. PTR Prentice Hall, Upper Saddle River, NJ, USA
31. Yoo TS, Selig ET (1979) Dynamics of Vibratory–Roller compaction. J Geotech Eng Div 105(10):1211–1231. https://doi.org/10.1061/AJGEB6.0000867